

Micromachined two-axis water-immersible scanning mirror using torsional and bending hinges

Shuangliang Li^{✉,*}, Xiaoyu Duan, and Jun Zou*

Texas A&M University, Department of Electrical and Computer Engineering,
College Station, Texas, United States

Abstract. We report a two-axis water-immersible microscanning mirror using torsional and bending biaxially oriented polyethylene terephthalate hinges. Two different designs based on a four- or single-coil electromagnetic actuator are investigated. A micromachining-based fabrication process is developed to enable high patterning resolution and alignment accuracy and to reduce the amount of manual assembly. With a torsional hinge, the fast axis has a resonance frequency of 300 to 500 Hz in air and 200 to 400 Hz in water. With a bending hinge, the slow axis has a resonance frequency of 60 to 70 Hz in air and 20 to 40 Hz in water. 2D B-scan and 3D volumetric ultrasound microscopy are demonstrated using the hybrid-hinge scanning mirror. The ability of scanning the slow axis at DC or very low frequencies allows a dense raster scanning pattern to be formed for improving both the imaging resolution and field of view. © *The Authors*. Published by SPIE under a Creative Commons Attribution 4.0 International License. Distribution or reproduction of this work in whole or in part requires full attribution of the original publication, including its DOI. [DOI: [10.1117/1.JOM.1.4.044001](https://doi.org/10.1117/1.JOM.1.4.044001)]

Keywords: water-immersible microscanning mirror; torsional and bending hinges; ultrasound microscopy; photoacoustic microscopy.

Paper 21010 received Jun. 6, 2021; accepted for publication Oct. 4, 2021; published online Oct. 28, 2021.

1 Introduction

Recently, microelectromechanical systems (MEMS) scanning mirrors have been developed to provide fast scanning of light beams in air for a number of optical applications, such as light detection and ranging,^{1,2} variable optical attenuator,³ fluorescence microscopy,⁴ and optical endoscopy.⁵ The MEMS scanning mirrors can be driven by different actuation mechanisms, such as electrostatic, electrothermal, piezoelectric, electromagnetic, and even hybrid modes.^{6,7} Further extending their applications in acoustic imaging, water-immersible microscanning mirrors (WIMSMs) also have been investigated to steer focused optical and ultrasound beams under water (the most commonly used coupling medium for ultrasound propagation).^{8–12} Different from conventional MEMS scanning mirror designs (for operation in air), flexible polymer hinges are used in the WIMSMs to resist the possible shock damage in a liquid environment. In addition, the WIMSMs are usually driven by electromagnetic actuators, which do not require high voltages can be easily made water-proof.

To achieve high imaging resolution, a dense 2D raster scanning pattern is desired, which requires the fast and slow axes to operate at two very different frequencies (e.g., 100s of Hz versus several Hz). To obtain the maximal scanning range, the two scanning axes need to be driven at a frequency near their mechanical resonance. Therefore, the resonance frequencies of the fast and slow axes should be made different as much as possible. In current WIMSMs, the two torsional hinges (one for fast axis and the other one for slow axis) are usually made of the same (polymer) material, such as biaxially oriented polyethylene terephthalate (BoPET) or polydimethylsiloxane.⁹ Even with different geometric designs, a large resonance-frequency ratio still cannot be readily obtained. To address this issue, a hybrid hinge structure made of BoPET and a soft elastomer nanocomposite was developed.¹³ With a much lower Young's modulus (e.g., several MPa), the elastomer hinge reduced the resonance frequency of the slow axis down to <1 Hz, while that of the BoPET hinge for the fast axis still remained at 100s of Hz. However,

*Address all correspondence to Shuangliang Li, slli940922@tamu.edu; Jun Zou, junzou@tamu.edu

the low stiffness of the torsional elastomer hinge could be more susceptible to mirror plate vibrations. Also handling two different hinge materials complicates the mirror fabrication and assembly.

Previously, we investigated a new hybrid hinge design based on different deformation (torsional and bending) modes.¹⁴ Specifically, the (stiffer) torsional hinge provides a high resonance frequency for the fast axis, whereas the (softer) bending hinge creates a low resonance frequency and enlarges the scanning range for the slow axis. By combining the torsional and bending modes, highly different driving frequencies of the fast and slow axes can be achieved with single (BoPET) hinge material. In this paper, we report two new designs of miniaturized WIMSMs with both torsional and bending hinges, which are driven by a four- or single-coil electromagnetic actuator, respectively. For demonstration, two prototype scanning mirrors (one with a four-coil and the other one with a single-coil actuator) have been designed, fabricated, and characterized. Their scanning performances were evaluated and compared. The four-coil design provides better scanning performance, whereas the single-coil one is more compact with simpler wiring. Using the new scanning mirror, scanning ultrasound microscopy has also been conducted.

2 Design

Figure 1 shows the schematic design of the micromachined water-immersible scanning mirror with torsional and bending hinges. The mirror plate is supported on the inner frame with two torsional hinges, which forms the fast axis. The inner frame is attached onto the outer frame with two bending hinges, which forms the slow axis. Two pairs of permanent magnets are bonded on the backside of the mirror plate. One pair of magnets is inversely magnetized to create a torque

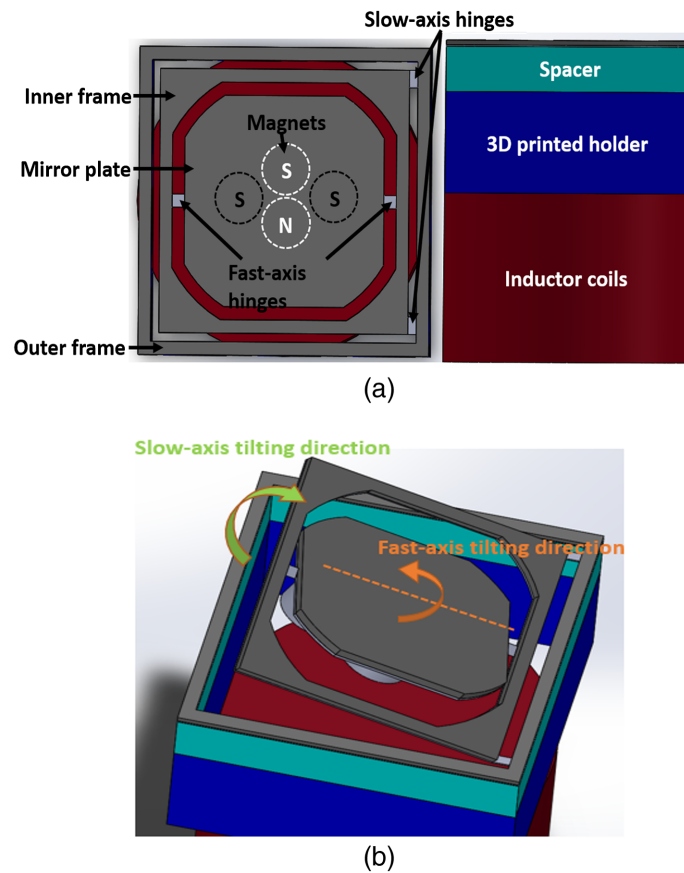


Fig. 1 (a) Schematic top and side views of the water-immersible scanning mirror with torsional and bending hinges. (b) Illustration of the deformation modes of the fast and slow axes (driven by single inductor coil).

for actuating the fast axis (with two torsional hinges). The other pair has the same polarity to create a pushing or pulling force for actuating the slow axis (with two bending hinges). In this way, the inductor coil(s) can be driven with currents of the same polarity, which works for both multi-coil or single-coil magnetic actuator designs. Because the two pairs of magnets are placed close to each other, there will be interaction of (fringing) magnetic fields between them. However, because the magnetic actuation is achieved with the magnetic field flux that is perpendicular to the magnet surface, such influence on the scanning performance should be small. The entire mirror plate structure is fixed onto a 3D printed holder (with one or multiple inductor coils). A spacer structure is used to set the gap between the permanent magnets and the inductors coil(s) for the proper functioning of the scanning mirror. If the gap is too small, the attractive (magnetostatic) force between the core of inductor coil(s) and permanent magnets could become strong enough to pull-in the bending hinges and prevent the operation of the slow axis. However, a large gap will reduce the strength of the magnetic field from the inductor coil, resulting in higher driving currents and lower energy efficiency.

For demonstration, two prototype scanning mirrors with an overall lateral dimension of $7 \times 7 \text{ mm}^2$ and $5 \times 5 \text{ mm}^2$ were designed, fabricated, and characterized. Their main design parameters are listed in Tables 1 and 2, respectively. For comparison, the 7×7 -mm scanning mirror is driven by four (smaller) inductor coils connected in parallel. Their arrangement matches that of the four magnets on the mirror plate to maximize the driving efficiency. To maintain its compactness, the 5×5 -mm one is driven by a single (larger) inductor coil. Because the fast and slow axes are supported by different torsion and bending hinges, their resonance frequencies vary significantly. As a result, their mechanical coupling will be well suppressed via the dynamic filtering effect,¹¹ which makes it possible to drive them simultaneously even with a single inductor coil. To facilitate the design, the resonance frequencies (i.e., the eigenfrequencies) of the fast and slow axes in both air and water were simulated with COMSOL Multiphysics[®]. The main material properties used in the simulation are listed in Table 3. Figure 2 shows the normalized displacement amplitude of the two axes working at their resonance frequencies. For the 7×7 -mm mirror, the resonance frequencies of the fast and slow axes in air are 307 and 54 Hz, respectively. In water, they are reduced to 223 and 39 Hz, respectively. For the 5×5 -mm mirror, the resonance frequencies of the fast and slow axes in air are 473 and 58 Hz, respectively. In water, they are reduced to 406 and 31 Hz, respectively.

Table 1 Main design of parameters for the 7×7 -mm mirror.

| 7×7 mirror | Fast axis | Slow axis |
|---|--|--|
| Hinge size ($l \times w \times t$) | $0.3 \times 0.36 \times 0.07 \text{ mm}^3$ | $0.2 \times 0.24 \times 0.07 \text{ mm}^3$ |
| Rotational part ($l \times w$) | $4.8 \times 4.8 \text{ mm}^2$ | $6 \times 6 \text{ mm}^2$ |
| Permanent magnets distance (mm) | 1.6 | 2.8 |
| The mirror size ($l \times w \times t$) | $7 \times 7 \times 0.2 \text{ mm}^3$ | |
| Magnet size ($d \times h$) | $1.6 \times 0.8 \text{ mm}^2$ | |

Table 2 Main design of parameters for the 5×5 -mm mirror.

| 5×5 mirror | Fast axis | Slow axis |
|---|---|--|
| Hinge size ($l \times w \times t$) | $0.1 \times 0.2 \times 0.07 \text{ mm}^3$ | $0.2 \times 0.08 \times 0.07 \text{ mm}^3$ |
| Rotational part ($l \times w$) | $3.6 \times 3.6 \text{ mm}^2$ | $4.1 \times 4.1 \text{ mm}^2$ |
| Permanent magnets distance (mm) | 1.6 | 1.6 |
| The mirror size ($l \times w \times t$) | $5 \times 5 \times 0.2 \text{ mm}^3$ | |
| Magnet size ($d \times h/2$) | $(1.6 \times 0.8)/2 \text{ mm}^2$ | |

Table 3 Main material properties used in COMSOL simulation.

| | |
|-------------------------------|-----------------------|
| Hinge Young's modulus (E) | 2.95 GPa |
| Hinge shear modulus (G) | 1.53 GPa |
| Hinge Poisson ratio | 0.38 |
| Magnet density | 7.5 g/cm ³ |

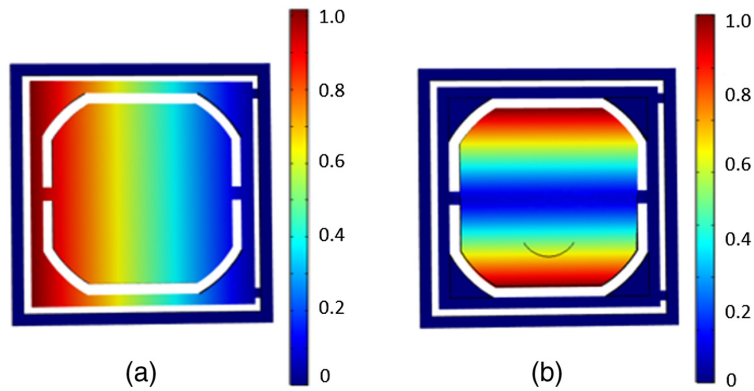


Fig. 2 Simulated displacement amplitude at the eigenfrequency of (a) the slow axis (b) the fast axis.

3 Fabrication and Assembly

Figure 3 shows the fabrication processes of the scanning mirror with torsional and bending hinges. First, a 20-nm-thick chrome layer (as an adhesion promoter) was deposited on a 70- μm -thick BoPET film [Fig. 3(a)], which was bonded onto a 200- μm -thick silicon wafer [Fig. 3(b)]. Second, a 20/200-nm-thick chrome/copper seed layer was deposited on the unbonded side of the BoPET film. A 600-nm-thick nickel layer was electroplated to serve as the etch mask for reactive ion etching of BoPET [Fig. 3(c)]. Third, a 300-nm aluminum layer was evaporated and

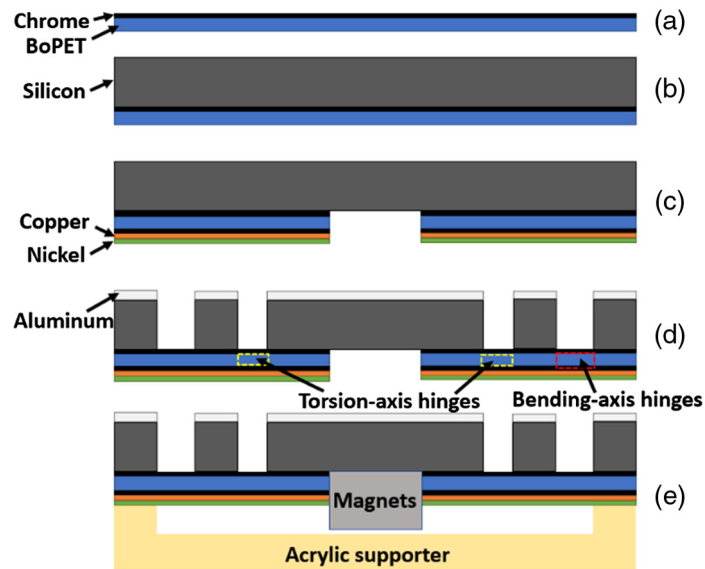


Fig. 3 (a)–(e) Fabrication and assembly process flow of the mirror plate.

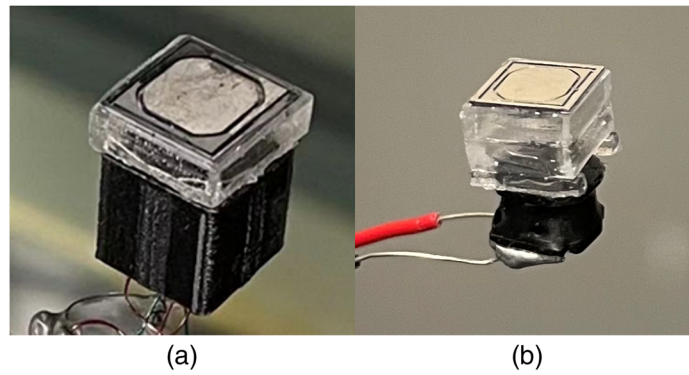


Fig. 4 Assembled prototypes of (a) 7×7 mm and (b) 5×5 mm scanning mirror.

patterned on the top side of silicon wafer to serve as the mask for cryogenic silicon etching¹⁵ and also as the reflective layer of mirror plate [Fig. 3(d)]. Next, four permanent magnet discs (D101-N52, K&J Magnetics) were attached underneath the fabricated mirror plate, which was bonded onto an acrylic spacer with epoxy [Fig. 3(e)]. To complete the 7×7 -mm mirror assembly, four inductor coils (5100-253604, Knowles) were inserted into a 3D-printed holder, which was bonded with the spacer [Fig. 4(a)]. For the 5×5 -mm mirror, four half magnet discs were used instead of four whole ones. A single inductor coil (74404054222, Würth Elektronik) was directly bonded on the bottom of the spacer without the 3D printed holder [Fig. 4(b)].

4 Characterization

A laser tracing method was carried out to characterize the mirror scanning performance (Fig. 5). The scanning mirror was fixed on a clamp at 45 deg downward. A collimated CW laser beam was incident horizontally onto the center of the mirror plate and reflected onto a ruler at a certain distance. Based on the distance between the ruler and the laser point on the mirror surface and the length of the trace, the optical tilting angle of the mirror plate was calculated.

The 7×7 -mm scanning mirror was characterized first. The frequency of the AC current was swept from 1 Hz to 1 kHz. Figure 6 shows the tilting angles versus frequency of the two axes in air and water, respectively. The resonance frequency is defined as the frequency where the maximum tilting angle was obtained. The frequency of the first one was defined as the resonance frequency of the slow axis, whereas the second one was defined as the resonance frequency of the fast axis. In air, the resonance frequencies of the fast and slow axes were determined as 311 and 66 Hz, respectively. In water, the resonance frequencies were reduced to 206 and 30 Hz, respectively. With bending hinges, significant increase in the viscous damping occurs on the slow axis in water, resulting in large reductions in its resonance frequency and quality factor, which makes it suitable for driving under DC or quasi-static conditions. During the testing, it was found out that the resonance frequencies of the two axes could drop slightly when the amplitude

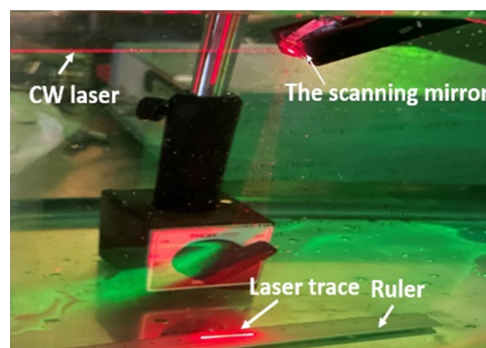


Fig. 5 The laser tracing setup.

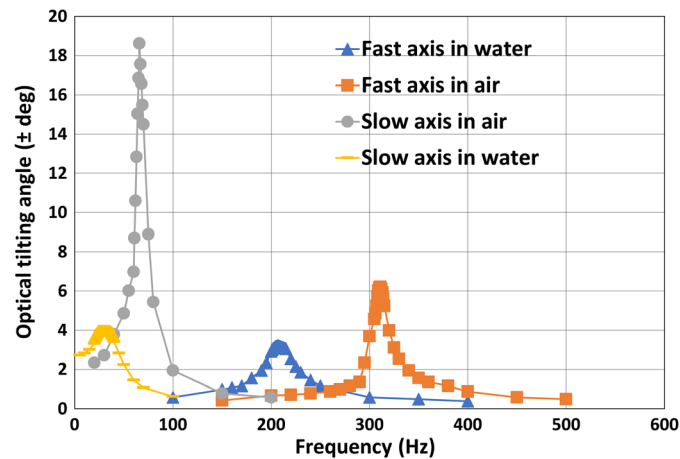


Fig. 6 Resonance frequency characterization of the fast and slow axes in the air and water for the 7×7 -mm scanning mirror. The amplitudes of the two AC driving currents (for the fast and slow axes) were 2.88 and 2.61 mA, respectively.

of the driving currents was increased. This phenomenon is due to the small openings on the mirror plate surface, which obstructs the air or water flow into and out of the fixture. When the mirror plate vibrates more under a larger current, it will subject to higher viscous damping, thereby reducing its resonance frequency. Therefore, for the characterization of the tilting angles with AC current driving, the driving frequencies were slightly adjusted to match the actual resonance frequencies at each current amplitude. In air, the resonance frequencies of the fast and slow axes were determined to be 311 to 322 Hz and 66 to 70 Hz, respectively. In water, the resonance frequencies were reduced to 205 to 216 Hz and 30 to 37 Hz, respectively.

Figure 7 shows the optical tilting angles at the adjusted resonance frequencies versus the AC driving current of the two axes in air and in water, respectively. Figure 8 shows the tilting angle of the slow axis versus the DC driving current in air and in water, respectively. At first, the optical tilting angles of the fast and slow axes increase almost linearly with the amplitude of the driving current and more slowly at larger currents. This is because when the mirror plate is tilted to a larger angle, more misalignments will occur between the magnet and the inductor coil. Figure 9(a) shows three representative laser scanning traces of the 7×7 -mm scanning mirror when the fast and slow axes were driven simultaneously by an AC and DC current, respectively. The AC current driving the fast axis was fixed at 3.3 mA at 206 Hz. The DC current of the slow axis was set to be -8.3 mA (-6.37 deg), 0 mA (0 deg), and 9.8 mA (5.54 deg), respectively. The tilting angle is slightly reduced at the two offset positions, which is mainly caused by the shifting of the resonance frequencies (from 206 Hz) at these two locations. Figure 9(b) shows the 2D

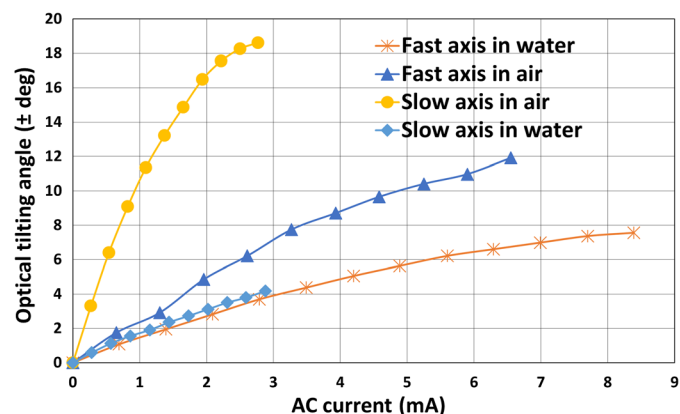


Fig. 7 Tilting angles of the fast and slow axes at the adjusted resonance frequencies for the 7×7 -mm scanning mirror.

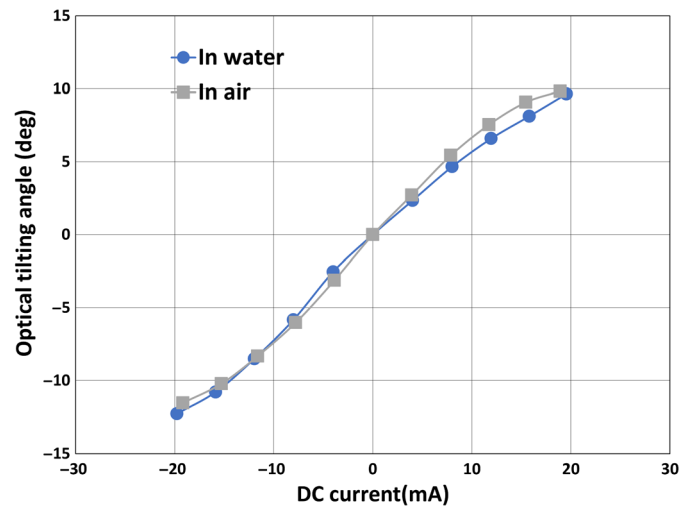


Fig. 8 The DC tilting angles of the slow axis in air and water for the 7×7 -mm scanning mirror.

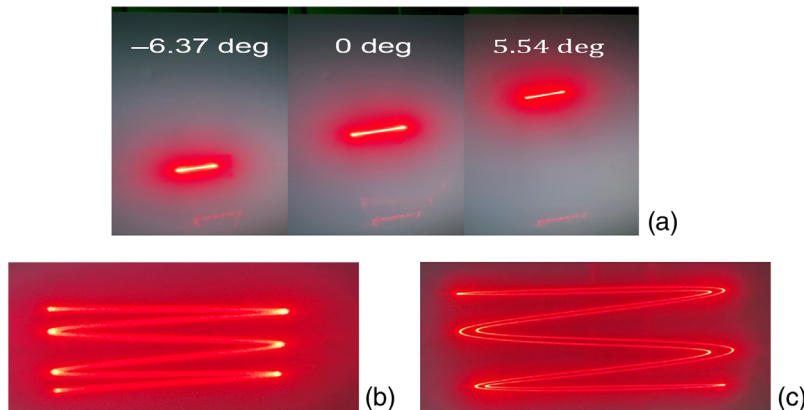


Fig. 9 Representative laser scanning traces generated by the 7×7 -mm scanning mirror with the fast and slow axes driven at different frequencies: (a) 206 Hz (fast) and DC (slow) in water, (b) 300 Hz (fast) and 50 Hz (slow) in air, and (c) 200 Hz (fast) and 40 (slow) in water.

raster scanning pattern in air when the fast and slow axes were driven at 300 and 50 Hz, respectively. Figure 9(c) shows the 2D raster scanning pattern in water when the fast and slow axes were driven at 200 and 40 Hz, respectively. For the 2D raster scanning pattern in water, there exists a shift between the forward and reverse scanning traces, which is due to a small phase shift caused by the slightly different damping conditions when the mirror plate rotates into and out of the mirror package (around the bending hinges) (Fig. 1). In the above three cases, the scanning traces remain stable and repeatable, indicating little mechanical coupling between the two axes due to their very different resonance frequencies of two axes.

The 5×5 -mm scanning mirror was characterized with the same procedure. Because the openings on the mirror surface are smaller, the viscous damping effect was even stronger than that of the 7×7 -mm scanning mirror. To alleviate the extra damping effect, two small vent holes were created on the two sides of the spacer. In air, the adjusted resonance frequencies of the fast and slow axes are 471 to 548 Hz and 64 to 67 Hz, respectively. In water, they were reduced to 376 to 401 Hz and 24 to 26 Hz, respectively. Figure 10 shows the optical tilting angles at the adjusted resonance frequencies versus the AC driving current of the two axes in air and in water, respectively. Figure 11 shows the tilting angles of the slow axis versus the DC driving current in air and in water, respectively. The tilting angles increase almost linearly with both AC and DC driving currents. However, compared with the 7×7 -mm scanning mirror, higher driving currents

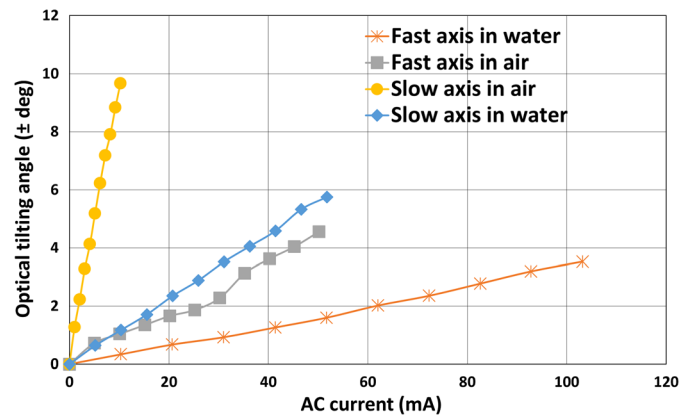


Fig. 10 Tilting angles of the fast and slow axes at the adjusted resonance frequencies for the 5×5 -mm scanning mirror.

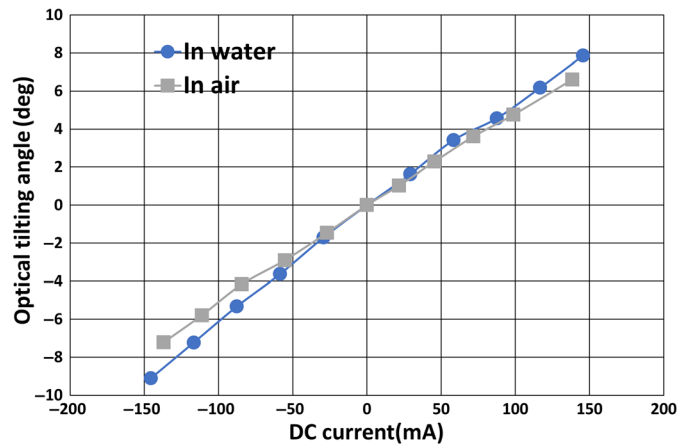


Fig. 11 The DC tilting angles of the slow axis in air and water for the 5×5 -mm scanning mirror.

are needed to obtain a similar tilting angle, which is due to the different designs of the electromagnetic actuator. For example, in order to obtain an optical tilting angle of 8 deg from the slow axis, the 7×7 -mm scanning mirror requires 20 mA of DC current for either of the two inductor coils, which is equal to a total current of 40 mA (Fig. 8). In contrast, the 5×5 -mm scanning mirror requires 150 mA of DC current for the single inductor coil to reach a similar optical tilting angle (Fig. 11). In the 7×7 -mm scanning mirror, four inductor coils are used to provide a one-to-one match with the four permanent magnets on the mirror plate. As a result, most of the magnetic flux from each coil can pass through the corresponding permanent magnet for maximizing the magnetic force generation. In the 5×5 -mm scanning mirror, a single (larger) inductor coil interacts with four (smaller) magnets, which results in weaker magnetic forces. However, the more uniform distribution of the magnetic flux from the single inductor coil contributes to a better linearity of the tilting angles. What is more, the single-coil design requires only two wire connections, instead of five or even eight for the four-coil design, and therefore, is helpful for simplifying the packaging.

5 Imaging Experiment

Pulse-echo ultrasound microscopy was conducted with the 7×7 -mm scanning mirror to demonstrate the underwater ultrasound beam steering capability. Figure 12 shows the experimental setup of the ultrasound imaging test. The scanning mirror was held by a clamp at 45 deg facing

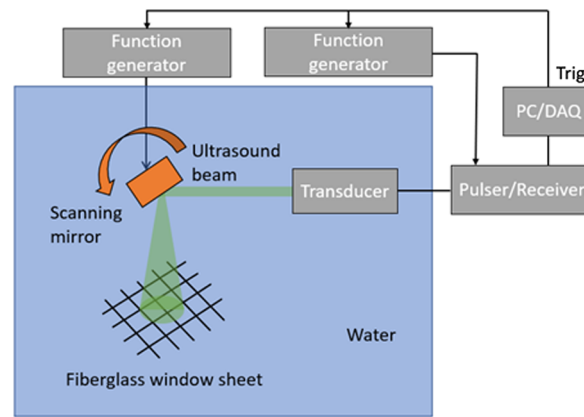


Fig. 12 Schematic of the pulse-echo ultrasound microscopy setup.

down. The 25-MHz ultrasound transducer (V376, Olympus, 31.75-mm focal length) was fixed horizontally at a distance about 6 mm. A fiberglass window screen sheet was placed underneath of the scanning mirror at a distance about 25 mm, serving as the imaging target. The ultrasound signal transception of the transducer was controlled by a pulser/receiver (5037PR, Olympus). The pulser/receiver was triggered by a function generator at 12.36 kHz. The fast and slow axes of the scanning mirror were driven simultaneously by a two-channel function generator. A data acquisition (DAQ) card (PCI 6251, National Instruments) was used to record the ultrasound echo signals for image reconstruction. To synchronize the operation of the scanning mirror and the pulser/receiver, the function generator and the pulser/receiver were both triggered by the DAQ card. The fast axis of the scanning mirror was driven by an 8.5-mA AC current at 206 Hz. The slow axis was driven by a 10-mA (sinusoidal) AC current at 0.125 Hz. This creates a field view of $8.5 \times 7.5 \text{ mm}^2$ at a distance of 25 mm. Within each cycle of fast-axis scanning, there were 60 data points determined by the ratio between the ultrasound pulse repetition rate (12.36 kHz) and the frequency of the driving signal (206 Hz). Only 30 data points were utilized for the image reconstruction because of the two overlapped traces within each scanning cycle. For the slow axis, it consists of 1648 scanning cycles of the fast axis. Only 824 lines were utilized for the image reconstruction because of the two overlapped traces within each scanning cycle. As a result, a total number of 24,720 (30×824) data points were used for the image reconstruction.

The ultrasound image reconstruction followed a similar process previously reported.¹² The 24,720 scan points were arranged together to form a 3D data matrix. At each scan point, the transducer sent an ultrasound pulse and received the backscattered “A-line” echo signal. The “A-line” signals obtained at the corresponding 30 scan points along the fast axis were combined to reconstruct a 2D raw B-mode image. The grayscale of the pixels represents the echo signal intensity. The lateral location of each pixel is determined by the location of the corresponding scan points, whereas the axial location is determined by its travel time multiplied by sound velocity in water. Next, 2D synthetic aperture focusing technique was applied on each B-mode image, followed by a sector transformation based on the real dimensions. This process was repeated until all of the 824 B-mode images were formed. Finally, all the B-mode images were stacked together to form a 3D volumetric image.

Figure 13 shows a representative B-mode image and the reconstructed overall 3D image in Volview[®]. From the reconstructed ultrasound image, the width and spacing of fiberglass threads are determined to be $400 \mu\text{m}$ and 1.5 mm, respectively, which are close to the actual values. The edges of the ultrasound image do not appear as clear as the center region. This is because the fiberglass window sheet was placed on a flat surface, whereas the focal point of the ultrasound transducer was aligned to its center region. When the mirror plate is tilted to a larger angle, the work distance between the target and the ultrasound transducer will change, which could make the target out of focus. This issue can be addressed by fixing the fiberglass window screen onto a concave surface to make all the scan points remain inside the focal zone.

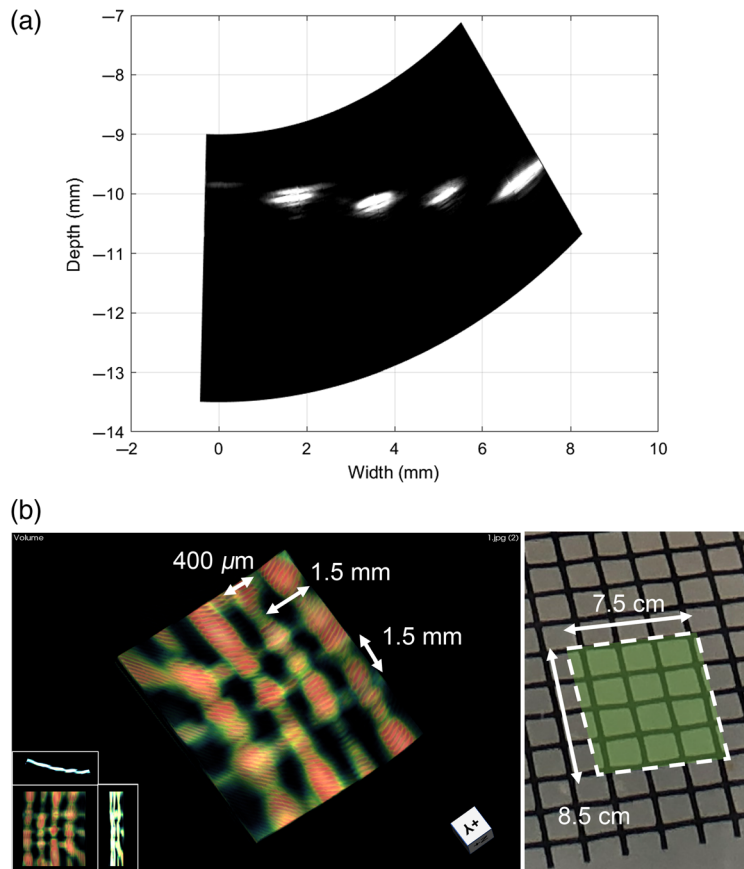


Fig. 13 Reconstructed (a) B-mode and (b) 3D image of a fiberglass window screen sheet.

6 Conclusion

In summary, a new hybrid torsional and bending polymer hinge structure has been investigated. By using the hybrid hinge structure, two micromachined WIMSMs driven by a four- or single-coil electromagnetic actuator have been demonstrated. The combination of the torsional and bending modes makes it possible to achieve very different driving frequencies of the fast and slow axes with single hinge material. Such feature is especially useful for generating a dense raster scanning pattern for scanning optical and acoustic microscopy. For demonstration, scanning ultrasound microscopy has also been conducted with the hybrid-hinge scanning mirror. In the future, the mirror packaging will be optimized to minimize the shift of the resonance frequencies caused by the amplitude-dependent viscous damping.

Acknowledgments

This work was supported in part by an award (No. CBET-2036134) from the National Science Foundation (NSF) and a grant (No. 1R01NS115581-01) from the National Institutes of Health (NIH) to J. Z.

References

1. D. Wang et al., "A low-voltage, low-current, digital-driven MEMS mirror for low-power LiDAR," *IEEE Sens. Lett.* **4**(8), 1–4 (2020).
2. D. Wang, S. J. Koppal, and H. Xie, "A monolithic forward-view MEMS laser scanner with decoupled raster scanning and enlarged scanning angle for micro-LiDAR applications," *J. Microelectromech. Syst.* **29**(5), 996–1001 (2020).

3. K. H. Koh, Y. Qian, and C. Lee, "Design and characterization of a 3D MEMS VOA driven by hybrid electromagnetic and electrothermal actuation mechanisms," *J. Micromech. Microeng.* **22**(10), 105031 (2012).
4. H. Yang et al., "Miniature fluorescence molecular tomography (FMT) endoscope based on a MEMS scanning mirror and an optical fiberscope," *Phys Med Biol.* **64**(12), 125015 (2019).
5. S. Luo et al., "Circumferential-scanning endoscopic optical coherence tomography probe based on a circular array of six 2-axis MEMS mirrors," *Biomed. Opt. Express* **9**, 2104–2114 (2018).
6. K. H. Koh and C. Lee, "A two-dimensional MEMS scanning mirror using hybrid actuation mechanisms with low operation voltage," *J. Microelectromechan. Syst.* **21**(5), 1124–1135 (2012).
7. K. H. Koh, T. Kobayashi, and C. Lee, "A 2-D MEMS scanning mirror based on dynamic mixed mode excitation of a piezoelectric PZT thin film S-shaped actuator," *Opt. Express* **19**, 13812–13824 (2011).
8. C. H. Huang and J. Yao, "A water-immersible 2-axis scanning mirror microsystem for ultrasound and photoacoustic microscopic imaging applications," *Microsyst. Technol.* **19**(4), 577–582 (2013).
9. J. Y. Kim et al., "Fast optical-resolution photoacoustic microscopy using a 2-axis water-proofing MEMS scanner," *Sci. Rep.* **5**(1), 7932 (2015).
10. S. Xu and J. Zou, "Two-axis water-immersible microscanning mirror for scanning optics and acoustic microscopy," *J. Micro/Nanolithogr. MEMS MOEMS* **15**(4), 045005 (2016).
11. S. Xu, X. Duan, and J. Zou, "A two-axis water-immersible microscanning mirror driven by single inductor coil through dynamic structural filtering," *Sens. Actuators A* **284**(12), 172–180 (2018).
12. S. Xu, S. Li, and J. Zou, "A micromachined water-immersible scanning mirror using BoPET hinges," *Sens. Actuators A* **298**, 111564 (2019).
13. X. Duan et al., "A two-axis water-immersible microscanning mirror using hybrid polymer and elastomer hinges," *Sens. Actuators A* **312**, 112108 (2020).
14. X. Duan and J. Zou, "A two-axis water-immersible microscanning mirror (WIMSM) using torsional and bending polymer hinges," *Proc. SPIE* **11697**, 116970A (2021).
15. P. E. Dyer, G. A. Oldershaw, and J. Sidhu, "CO₂ laser ablative etching of polyethylene terephthalate," *Appl. Phys. B* **48**(6), 489–493 (1989).

Shuangliang Li received his BS degree in microelectronics science and engineering from East China Normal University in 2017. He is currently pursuing his PhD in the Department of Electrical and Computer Engineering at Texas A&M University. His current research is mainly on MEMS scanning mirrors design and fabrication.

Xiaoyu Duan received her BS degree in microelectronic and optoelectronic engineering from Sun Yat-sen University, Guangzhou, China, in 2015. She is currently a PhD student in the Department of Electrical Engineering at Texas A&M University. Her major research interests involve underwater optical and acoustic dual-modal communication and ranging devices.

Jun Zou received his PhD in electrical engineering from the University of Illinois at Urbana-Champaign in 2002. In 2004, he joined in the Department of Electrical and Computer Engineering at Texas A&M University, where he is currently a full professor. His current research interests lie in the development of micro- and nano-opto-electro-mechanical devices and systems for biomedical imaging and sensing applications. He is a senior member of IEEE and SPIE and a member of OSA.